Catalysis Today 442 (2024) 114910

Contents lists available at ScienceDirect

Catalysis Today

journal homepage: www.elsevier.com/locate/cattod

The direct synthesis of H_2O_2 and *in situ* oxidation of methane: An investigation into the role of the support

Fenglou Ni [a,1], Richard J. Lewis [a,*], Ángeles López-Martín [a], Louise R. Smith [a], David J. Morgan [a,b], Thomas E. Davies [a], Stuart H. Taylor [a], Graham J. Hutchings [a,*]

[a] Max Planck–Cardiff Centre on the Fundamentals of Heterogeneous Catalysis FUNCAT, Cardiff Catalysis Institute, School of Chemistry, Cardiff University, Cardiff CF24 4HQ, United Kingdom

[b] Harwell XPS, Research Complex at Harwell (RCaH), Didcot OX11 0FA, United Kingdom

ARTICLE INFO

Keywords:
Methane oxidation
Hydrogen peroxide
Green chemistry
Gold
Palladium

ABSTRACT

The selective oxidation of methane to methanol, using H_2O_2 generated *in situ* from H_2 and O_2 has been investigated using bimetallic gold-palladium catalysts, prepared via an industrially relevant wet co-impregnation protocol on a range of zeolite and metal oxide supports. The choice of catalyst support was found to drastically influence catalyst performance, through control of both nanoparticle dispersion and Pd speciation. Notably in the case of those formulations prepared on metal oxides a direct correlation between catalytic performance towards H_2O_2 synthesis and methane valorisation exists, whereas in the case of the zeolitic-based analogues, no clear correlation could be drawn between activity towards individual reaction pathways.

1. Introduction

The oxidative valorisation of methane to methanol represents a long-standing challenge of catalysis, with global demand for this platform chemical exceeding 20 billion gallons/annum [1]. Currently, large-scale methanol production is reliant on the syngas route, where methane is first converted to CO and H_2 via steam (or dry) reforming. However, the energy-intensive conditions required by current industrial methanol synthesis routes (200–300 °C and up to 100 bar pressure), and the propensity for CO_2 production, via the water-gas-shift reaction, which effectively limits efficient CO utilisation, has led to long-standing interest in alternative approaches to methanol production [2]. To this end, the selective oxidation of methane via the *in situ* synthesis of H_2O_2 has been an area of considerable interest, requiring reaction temperatures far lower than current industrial technologies or alternative approaches which rely on O_2 as the terminal oxidant [3–6]. Indeed, the *in situ* route can be considered to be more economically viable than alternative approaches that utilise commercial H_2O_2, an approach which itself has seen significant interest, [7,8] with the cost of the preformed oxidant comparable to that of methanol. However, despite significant advancements in recent years, [9] there is still a need to improve catalytic performance if the *in situ* approach is ever to reach parity with current industrial technologies.

Bimetallic AuPd nanoalloy catalysts are widely considered among the state of the art for the direct synthesis of H_2O_2 as well as a range of oxidative transformations, [10] including those reliant on the *in situ* generation of the oxidant [9,11,12]. This has largely been attributed to the ability of Au incorporation to weaken the interaction between the metal surface and H_2O_2. Consequently, the dissociation of the HO-OH bond is inhibited and the desorption of the product is promoted [13–15]. Importantly, a growing body of literature has demonstrated that in addition to promoting H_2O_2 desorption the alloying of Au with Pd also results in an increased release of highly reactive oxygen-based radicals (ROS, •OOH, •OH and $\bullet O_2^-$), which are generated as reaction intermediates during H_2O_2 synthesis [15–17]. With the activation of methane over AuPd surfaces known to proceed through hydrogen abstraction and the termination of the resulting methyl radical via interaction with transient oxygen species leading to oxygenate synthesis, it is possible to draw a direct correlation between methane oxidation and the rate of ROS formation. The reader is directed to the comprehensive work by Stach and co-workers for an in-depth discussion of the kinetics and mechanism of H_2O_2-mediated methane upgrading over AuPd surfaces [3,8].

In an attempt to improve the efficient utilisation of the oxidant and

* Corresponding authors.
E-mail addresses: LewisR27@cardiff.ac.uk (R.J. Lewis), Hutch@cardiff.ac.uk (G.J. Hutchings).
[1] These authors contributed equally to this work.

https://doi.org/10.1016/j.cattod.2024.114910

Available online 1 July 2024

overcome diffusion limitations, Jin *et al.* have recently investigated the role of organosilane modification of AuPd@ZSM-5 catalysts for the oxidative valorisation of methane via *in situ* H_2O_2 synthesis. The presence of the hydrophobic oganosilane layer was found to both promote localised concentration of reagents at active sites, improving H_2O_2 synthesis rates, as well as confining the synthesised oxidant near the AuPd species for use in methane activation.

The choice of catalyst support has been widely reported as a crucial factor in determining performance towards the direct synthesis of H_2O_2, a key reaction step in the *in situ* valorisation of methane, controlling the degree of nanoalloy formation as well as particle morphology and active site dispersion [18,19]. Notably, Ntainjua *et al.* have reported a strong correlation between the isoelectric point of the support (*i.e.* the pH at which the surface has zero net charge and an indicator of basicity/acidity), and H_2O_2 synthesis activity (and selectivity), particularly for AuPd catalysts prepared via a wet co-impregnation methodology [19]. With these earlier studies in mind, we now investigate the role of catalyst support for the oxidative valorisation of methane to liquid oxygenates using *in situ* generated H_2O_2, utilising a wide range of both oxide and zeolitic carriers for AuPd nanoparticles. Notably, for this study, we have chosen to utilise an excess chloride (0.58 M HCl) wet co-impregnation route to catalyst synthesis, with this procedure previously identified to offer improved efficacy compared to alternative impregnation-based protocols, owing to a combination of improved control of nanoparticle size as well as compositional uniformity [20,21].

2. Experimental

2.1. Catalyst preparation

Bimetallic AuPd catalysts have been prepared (on a weight basis), on a range of supports, by an excess chloride co-impregnation procedure, based on a methodology previously reported in the literature, which has been shown to improve the dispersion of metal species, particularly Au [20]. The procedure to produce 0.5 %Au–0.5 %Pd/TiO_2 (2 g) is outlined below, with a similar methodology utilized for all catalysts.

Aqueous acidified $PdCl_2$ solution (1.667 mL, 0.58 M HCl, [Pd] = 6.0 $mgmL^{-1}$, Merck) and aqueous $HAuCl_4{\cdot}3\,H_2O$ solution (0.8263 mL, [Au] = 12.25 $mgmL^{-1}$, Strem Chemicals) were mixed in a 50 mL round-bottom flask and heated to 65 °C with stirring (1000 rpm) in a thermostatically controlled oil bath, with total volume fixed to 16 mL using H_2O (HPLC grade, Fischer Scientific). Upon reaching 65 °C, TiO_2 (1.98 g, Degussa, P25) was added over the course of 5 min with constant stirring. The resulting slurry was stirred at 65 °C for a further 15 min, following this the temperature was raised to 95 °C for 16 h to allow for complete evaporation of water. The resulting solid was ground prior to a reductive heat treatment (5 %H_2/Ar, 500 °C, 4 h, 10 °C min^{-1}).

In the case of those materials prepared on ZSM-5 support materials the support (NH_4-ZSM-5, Zeolyst) was calcined in flowing air (450 °C, 6 h, 3 °C min^{-1}) according to our previous study [22].

2.2. Catalyst testing

Note 1: For both H_2O_2 direct synthesis and degradation experiments the reactor temperature was controlled using a HAAKE K50 bath/circulator using an appropriate coolant. Reactor temperature was maintained at 2 °C ±0.2°C throughout the course of the H_2O_2 synthesis and degradation reaction.

Note 2: The conditions used within this work for H_2O_2 synthesis and degradation have previously been investigated, with the use of sub-ambient reaction temperatures, CO_2 reactant gas diluent and a methanol co-solvent identified as key to maintaining high catalytic efficacy towards H_2O_2 production [23].

Note 3: In all cases, reactions were run multiple times, over multiple batches of catalyst, with the data being presented as an average of these experiments.

2.3. Direct synthesis of H_2O_2

Hydrogen peroxide synthesis was evaluated using a Parr Instruments stainless steel autoclave with a nominal volume of 100 mL and a maximum working pressure of 2000 psi. To test each catalyst for H_2O_2 synthesis, the autoclave was charged with catalyst (0.01 g) and solvent (5.6 g methanol and 2.9 g H_2O, Fischer Scientific, HPLC standard). The charged autoclave was then purged three times with 5 %H_2/CO_2 (100 psi) before filling with 5 %H_2/CO_2 to a pressure of 420 psi, followed by the addition of 25 %O_2/CO_2 (160 psi). The reaction was conducted at a temperature of 2 °C, for 0.5 h with stirring (1200 rpm). Reactant gases were not continuously supplied. H_2O_2 productivity was determined by titrating aliquots of the final solution after reaction with acidified $Ce(SO_4)_2$ (0.0085 M) in the presence of ferroin indicator. Catalyst productivities are reported as $mol_{H2O2}kg_{cat}^{-1}h^{-1}$.

Catalytic conversion of H_2 and selectivity towards H_2O_2 were determined using analysis by a Varian 3800 GC fitted with TCD and equipped with a Porapak Q column.

H_2 conversion (Eq. 1) and H_2O_2 selectivity (Eq. 2) are defined as follows:

$$H_2\text{Conversion}(\%) = \frac{\text{mmol}_{H2\ \ (t(0))} - \text{mmol}_{H2\ \ (t(1))}}{\text{mmol}_{H2\ \ (t(0))}} \times 100 \quad (1)$$

$$H_2O_2\text{Selectivity}(\%) = \frac{H_2O_2\text{detected(mmol)}}{H_2\text{consumed(mmol)}} \times 100 \quad (2)$$

The catalytic activity toward H_2O_2 synthesis was found to be consistent to within ±3 % on the basis of multiple reactions.

2.4. Degradation of H_2O_2

Catalytic activity towards H_2O_2 degradation (the sum of H_2O_2 decomposition and hydrogenation pathways), was determined in a similar manner to the direct synthesis activity of a catalyst. The autoclave was charged with methanol (5.6 g, Fischer Scientific, HPLC standard), H_2O_2 (50 wt% 0.68 g, Merck), H_2O (2.22 g, Fischer Scientific HPLC standard) and catalyst (0.01 g), with the solvent composition equivalent to a 4 wt% H_2O_2 solution. From the solution, 2 aliquots of 0.05 g were removed and titrated with acidified $Ce(SO_4)_2$ solution using ferroin as an indicator to determine an accurate concentration of H_2O_2 at the start of the reaction. The autoclave was pressurised with 5 %H_2/CO_2 (420 psi). The reaction was conducted at a temperature of 2 °C, for 0.5 h with stirring (1200 rpm). After the reaction was complete the catalyst was removed from the reaction mixture and two aliquots of 0.05 g were titrated against the acidified $Ce(SO_4)_2$ solution using ferroin as an indicator. The degradation activity is reported as $mol_{H2O2}kg_{cat}^{-1}h^{-1}$.

The catalytic activity toward H_2O_2 synthesis was found to be consistent to within ±2 % on the basis of multiple reactions.

2.5. Methane oxidation using in situ synthesised H_2O_2

The oxidation of methane was carried out using a Parr stainless steel autoclave with a nominal volume of 50 mL reactor and a maximum working pressure of 2000 psi. To evaluate catalytic activity towards the oxidative valorisation of methane, the autoclave was charged with catalyst (0.027 g) and solvent (10 g H_2O, Fischer Scientific, HPLC grade). Subsequently, the reactor was purged with methane (100 psi) and then charged with pure H_2, N_2, O_2 and CH_4 such that the total pressure equalled 435 psi. The gas phase composition was 0.8 % H_2/ 1.6 % O_2/ 76.7 % CH_4/ 20.8 % N_2 to ensure the mixture was outside of the explosive limits. The autoclave was then heated to the desired reaction temperature (50 °C), once at the set temperature, the reaction solution was stirred at 1500 rpm for 0.5 h. After the reaction was complete the stirring was stopped and the temperature was reduced to 10 °C using ice in order to minimize the loss of volatile products. Gaseous samples were analysed via gas chromatography (Varian-GC,

Table 1
Catalytic activity of AuPd catalysts towards the direct synthesis and subsequent degradation of H_2O_2, as a function of catalyst support.

Catalyst	Productivity / $mol_{H2O2}kg_{cat}^{-1}h^{-1}$	H_2O_2 / wt %	H_2 Con. / %	H_2O_2 Sel. / %	Initial reaction rate / $mmol_{H2O2}mmol_{metal}^{-1}h^{-1}$*	Degradation / $mol_{H2O2}kg_{cat}^{-1}h^{-1}$
0.5 %Au-0.5 %Pd/TiO_2	95	0.19	21	31	2.22×10^3	237
0.5 %Au-0.5 %Pd/Al_2O_3	84	0.17	25	23	1.98×10^3	204
0.5 %Au-0.5 %Pd/Ga_2O_3	70	0.14	12	43	2.64×10^3	106
0.5 %Au-0.5 %Pd/SiO_2	47	0.10	11	32	8.85×10^2	112
0.5 %Au-0.5 %Pd/CeO_2	40	0.08	15	18	1.01×10^3	167
0.5 %Au-0.5 %Pd/Nb_2O_5	40	0.08	9	31	9.26×10^2	11
0.5 %Au-0.5 %Pd/ZrO_2	10	0.02	3	97	1.08×10^3	129
0.5 %Au-0.5 %Pd/Zeolite Beta	119	0.24	24	36	3.10×10^3	170
0.5 %Au-0.5 %Pd/MCM-41	77	0.16	64	9	2.27×10^3	288
0.5 %Au-0.5 %Pd/TS-1	76	0.16	40	14	1.26×10^3	391
0.5 %Au-0.5 %Pd/Zeolite A	56	0.12	33	12	1.67×10^3	87
0.5 %Au-0.5 %Pd/Zeolite Y	18	0.04	5	29	7.46×10^2	323
0.5 %Au-0.5 %Pd/ZSM-5(23)	58	0.12	25	17	1.29×10^3	368
0.5 %Au-0.5 %Pd/ZSM-5(30)	76	0.16	43	13	2.17×10^3	499
0.5 %Au-0.5 %Pd/ZSM-5(80)	31	0.06	59	4	1.01×10^3	579
0.5 %Au-0.5 %Pd/ZSM-5(280)	79	0.16	38	15	1.51×10^3	290

H_2O_2 direct synthesis reaction conditions: Catalyst (0.01 g), H_2O (2.9 g), MeOH (5.6 g), 5 %H_2/CO_2 (420 psi), 25 %O_2/CO_2 (160 psi), 0.5 h, 2 °C, 1200 rpm. **H_2O_2 degradation reaction conditions:** Catalyst (0.01 g), H_2O_2 (50 wt% 0.68 g) H_2O (2.22 g), MeOH (5.6 g), 5 %H_2/CO_2 (420 psi), 0.5 h, 2 °C 1200 rpm. * Initial reaction rate determined at a reaction time of 0.083 h.

equipped with a CPSIL5CB column (50 m, 0.33 mm internal diameter) fitted with a methanizer and flame ionization detector (FID)). The reaction mixture was filtered to remove the catalyst and analyzed by ^{1}H NMR, using a Bruker 500 MHz Ultrashield NMR spectrometer. All ^{1}H NMR samples were analysed against a calibrated insert containing tetramethylsilane (TMS) in deuterated chloroform (99.9 % D).

The catalytic activity toward methane oxidation was found to be consistent to within ±4 % on the basis of multiple reactions.

2.6. Characterisation

Investigation of the bulk structure of the materials was carried out using powder X-ray diffraction (XRD) on a (θ–θ) PANalyticalX'pert Pro powder diffractometer using a Cu Kα radiation source operating at 40 keV and 40 mA. Standard analysis was performed between 2θ values of 10–80° with the samples supported on an amorphous silicon wafer. Diffraction patterns of phases were identified using the ICDD database.

XPS measurements were performed on a Thermo Scientific K-Alpha$^+$ spectrometer using a monochromatic AlKα radiation source operating at 72 W (6 mA x 12 kV) which defines an analysis area of approximately 400 ×600 microns. An analyser pass energy of 150 eV was used for survey scans, and 50 eV for elemental regions, all samples were recorded using a dual ion-electron charge compensation detector, operating with an argon background pressure of *ca.*10^{-7} mbar. Samples were mounted by pressing on to silicone-free double-sided adhesive tape. Reported binding energies were referenced to a Si(2p) binding energy of 102.6 eV common for aluminosilicate materials, this was chosen as a more stable reference due to the low carbon concentrations on some of the materials leading to a greater deal of uncertainty in the C(1 s) peak position. Spectra were quantified using CasaXPS [22] using a Shirley-type background and an electron escape depth dependence based on the TPP-2 M equation and Scofield sensitivity factors to obtain surface compositions (atom %) of the different samples.

Brunauer Emmett Teller (BET) surface area measurements of oxide-supported catalysts were conducted using a Quadrasorb surface area analyser. A 5-point isotherm of each material was measured using N_2 as the adsorbate gas. Samples were degassed at 250 °C for 2 h prior to the surface area being determined by 5-point N_2 adsorption at −196 °C, and data analysed using the BET method. Corresponding analysis of zeolitic samples were collected on a Micromeritics 3Flex analyser. Samples (ca. 0.05 g) were degassed (250°C, 6 h) prior to analysis. Analyses were carried out at 77 K with P0 measured continuously. Free space was measured post-analysis with He. Pore size analysis was carried out using Micromeritics 3Flex software, applying a N_2-Cylindrical Pores-Oxide Surface DFT Model.

Note 4: Surface area measurements and porosimetry analysis of key samples are reported in Table S.1. A degree of surface area and pore volume loss was observed as for these samples after metal immobilisation and subsequent exposure to a reductive heat treatment.

Fourier-transform infrared spectroscopy (FTIR) was carried out with a Bruker Tensor 27 spectrometer fitted with a HgCdTe (MCT) detector and operated with OPUS software.

Note 5: FTIR analysis of the as-supplied zeolitic supports and corresponding catalytic samples are reported in Figure S.1 and reveals no discernible change in the observed positions of the absorption bands associated with the zeolitic frameworks.

Total metal leaching from supported catalysts was quantified through the analysis of post-reaction solutions using an Agilent 7900 ICP-MS equipped with an I-AS auto-sampler using 5-point calibration using certified reference materials from Perkin Elmer and certified internal standards from Agilent. All calibrants were matrix matched.

Aberration-corrected scanning transmission electron microscopy was performed using a probe-corrected Thermo Fisher Scientific Spectra 200 Cold-FEG operating at 200 kV. The instrument was equipped with a HAADF detector, and the imaging was done at a probe current of 120 pA and convergence angle of 30 mrad. Samples were dry dispersed onto 300 mesh copper grids coated with a holey carbon film. Energy-dispersive X-ray (EDX) mapping was performed using a Super-X G2 detector at a

dwell time of 25 μs. All images and EDX data were processed using Velox software.

3. Results and discussion

Numerous previous studies have identified that the choice of nanoparticle support can have a significant effect on catalytic performance towards the direct synthesis of H_2O_2, dictating the degree of alloy formation, nanoparticle composition and metal dispersion [18,19]. Notably, we have previously identified that the isoelectric point of the support (*i.e.,* the pH at which the surface has zero net charge, and an indication of catalyst acidity/basicity) may also be a crucial factor in determining catalytic activity towards the direct synthesis of H_2O_2, with supports of lower isoelectric points typically offering increased rates of H_2O_2 production [19]. However, such a relationship between the isoelectric point of the support and catalytic performance has also been found to be highly dependent on the means of catalyst synthesis, with materials prepared via an excess-chloride co-impregnation procedure influenced to a lesser degree by this metric [18] than analogous materials prepared by a conventional wet co-impregnation route in the absence of excess-chloride [19].

Therefore, with a focus on catalyst formulations prepared via the excess-chloride impregnation route and under reaction conditions that have been previously optimised for H_2O_2 production [23] our initial studies investigated the performance of AuPd nanoalloys, immobilised onto a range of common oxide and zeolitic supports for the direct synthesis and subsequent degradation of H_2O_2 (Table 1). A strong dependency is observed between catalytic activity towards H_2O_2 production and the choice of support, with the enhanced activity of the Zeolite-Beta (119 $mol_{H2O2}kg_{cat}^{-1}h^{-1}$), TiO_2 (95 $mol_{H2O2}kg_{cat}^{-1}h^{-1}$) and Al_2O_3 (84 $mol_{H2O2}kg_{cat}^{-1}h^{-1}$) supported catalysts clear. The improved performance of these formulations is further evidenced through the determination of initial reaction rates, measured at a reaction time (5 min), where the reaction is not considered to be limited by reagent availability and there is assumed to be negligible contribution from competitive degradation (hydrogenation and decomposition) pathways (Table 1). Interestingly, earlier studies have identified the limited activity of Al_2O_3-supported AuPd catalysts towards the direct synthesis of H_2O_2, when prepared by a wet co-impregnation procedure (*i.e.* in the absence of the excess chloride used in this work). Indeed, Edwards *et al.* have reported the H_2O_2 synthesis activity of a 5 %AuPd/Al_2O_3 catalyst to be as low as 18$mol_{H2O2}kg_{cat}^{-1}h^{-1}$ when evaluated under identical conditions to that used in this study, approximately 6 times lower than that reported for the 1 %AuPd/Al_2O_3 reported herein, despite the significantly lower total metal loading of the latter formulation [24]. It is therefore clear that the route to catalyst preparation and in particular the use of excess-chloride (0.58 M HCl) and a reductive thermal treatment can significantly improve catalytic reactivity. Indeed, it is notable that the performance of the 0.5 %Au-0.5 %Pd/Al_2O_3 catalyst prepared in this work is similar to that offered by the well-studied TiO_2 supported analogue [20,21,23].

With the exception of the 0.5 %Au-0.5 %Pd/MCM-41, 0.5 %Au-0.5 %Pd/Zeolite-Beta and 0.5 %Au-0.5 %Pd/SiO_2 catalysts, subsequent evaluation of the as-synthesised catalysts by XRD (Figure S.2), does not indicate the presence of poorly dispersed metal species, with no reflections associated with either Au or Pd observed. However, it should be noted that such observations may be a result of the low loading of active metals (1 wt% total), rather than an indication of the absence of larger metal species. Notably, even in the case of the MCM-41, SiO_2 and Zeolite-Beta supported formulations the metal reflections observed at 2θ=38° (associated with the Au (111) plane) and 2θ=44° (associated with the Pd (200) plane), are relatively weak. Regardless, it is clear that, in particular, the performance of the 0.5 %Au-0.5 %Pd/Zeolite-Beta catalyst (119 $mol_{H2O2}kg_{cat}^{-1}h^{-1}$) is not limited by the poor dispersion which may be inferred by XRD analysis. Importantly, our XRD analysis of the zeolite-supported formulations, as well as subsequent FTIR evaluation (Figure S.1), does not indicate any clear loss in support structure, as a result of catalyst preparation and reductive heat treatment. These observations are perhaps unsurprising given the known high thermal and chemical stability of many of the zeolites selected for study. Indeed, in specific regard to the ZSM-5-based materials, Lu *et al.* have previously reported no significant loss in crystallinity with exposure to temperatures as high as 800 °C, far beyond that used within this study [25].

CO-DRIFTS analysis was subsequently employed to investigate the ability of catalyst support to dictate nanoparticle composition (Figure S.3). The DRIFTS spectra of all formulations were found to be dominated by Pd-CO stretching modes, with those signals within the higher wavenumber region of the spectra (approx. 2200–2000 cm^{-1}) attributed to CO linearly co-ordinated to high energy or low-coordination Pd sites (*i.e.*, edges or corners), while those centred at

Table 2
The role of the support in dictating Pd oxidation state, as determined by XPS analysis of as-prepared catalysts.

Catalyst	Pd: Au	Pd^{2+} : Pd^0	Productivity / $mol_{H2O2}kg_{cat}^{-1}h^{-1}$	Degradation / $mol_{H2O2}kg_{cat}^{-1}h^{-1}$
0.5 %Au-0.5 %Pd/TiO_2	3.2	0.8	95	237
0.5 %Au-0.5 %Pd/Al_2O_3	17.0	0.9	84	204
0.5 %Au-0.5 %Pd/Ga_2O_3	2.8	All Pd^{2+}	70	106
0.5 %Au-0.5 %Pd/SiO_2	1.67	n.d.	47	112
0.5 %Au-0.5 %Pd/CeO_2	2.3	All Pd^{2+}	40	167
0.5 %Au-0.5 %Pd/Nb_2O_5	0.4	All Pd^0	40	11
0.5 %Au-0.5 %Pd/ZrO_2	2.9	All Pd^0	10	129
0.5 %Au-0.5 %Pd/Zeolite-Beta	1.5	2.0	119	170
0.5 %Au-0.5 %Pd/MCM-41	1.0	0.7	77	288
0.5 %Au-0.5 %Pd/TS-1	n.d.	n.d.	76	391
0.5 %Au-0.5 %Pd/Zeolite A	1.3	1.5	56	87
0.5 %Au-0.5 %Pd/Zeolite Y	2.0	All Pd^0	18	323
0.5 %Au-0.5 %Pd/ZSM-5(23)	0.7	All Pd^0	58	368
0.5 %Au-0.5 %Pd/ZSM-5(30)	0.7	All Pd^0	76	499
0.5 %Au-0.5 %Pd/ZSM-5(80)	0.7	All Pd^0	31	579
0.5 %Au-0.5 %Pd/ZSM-5 (280)	0.4	All Pd^0	79	290

H_2O_2 direct synthesis reaction conditions: Catalyst (0.01 g), H_2O (2.9 g), MeOH (5.6 g), 5 %H_2/CO_2 (420 psi), 25 %O_2/CO_2 (160 psi), 0.5 h, 2 °C, 1200 rpm. **n.d:** not determined due to poor Pd signal.

Table 3
Catalytic activity of AuPd catalysts towards the oxidation of methane to methanol via *in situ* H_2O_2 production, as a function of catalyst support.

Catalyst	Products / μmol						CH_3OH Sel. / %	Oxygenates Sel. / %	Productivity / $\mu mol_{oxygenates} \mu mol_{metal}^{-1} h^{-1}$
	CH_3OH	CH_3OOH	HCOOH	CO_2	Total Products	Total Oxygenates			
0.5 %Au-0.5 %Pd/TiO_2	0.24	0.00	0.35	0.73	1.32	0.59	18	45	0.58
0.5 %Au-0.5 %Pd/Al_2O_3	0.10	0.00	0.24	0.86	1.20	0.34	12	28	0.34
0.5 %Au-0.5 %Pd/Ga_2O_3	0.14	0.00	0.24	0.46	0.84	0.38	17	45	0.38
0.5 %Au-0.5 %Pd/SiO_2	0.08	0.00	0.20	0.64	0.92	0.28	9	30	0.28
0.5 %Au-0.5 %Pd/CeO_2	0.10	0.00	0.12	0.17	0.39	0.22	26	56	0.22
0.5 %Au-0.5 %Pd/Nb_2O_5	0.15	0.00	0.11	0.42	0.68	0.26	22	38	0.26
0.5 %Au-0.5 %Pd/ZrO_2	0.04	0.00	0.09	0.40	0.53	0.13	8	25	0.13
0.5 %Au-0.5 %Pd/Zeolite-Beta	0.11	0.00	0.35	0.58	1.04	0.46	11	44	0.47
0.5 %Au-0.5 %Pd/MCM41	0.05	0.00	0.00	0.68	0.73	0.05	7	7	0.05
0.5 %Au-0.5 %Pd/TS-1	0.06	0.00	0.28	1.02	1.36	0.34	4	25	0.35
0.5 %Au-0.5 %Pd/Zeolite A	0.06	0.00	0.29	0.95	1.30	0.35	5	27	0.37
0.5 %Au-0.5 %Pd/Zeolite Y	0.21	0.00	0.00	0.64	0.85	0.21	25	25	0.22
0.5 %Au-0.5 %Pd/ZSM-5(23)	0.15	0.00	0.00	0.56	0.71	0.15	21	21	0.16
0.5 %Au-0.5 %Pd/ZSM-5(30)	0.16	0.00	0.00	0.65	0.81	0.16	20	20	0.17
0.5 %Au-0.5 %Pd/ZSM-5(80)	0.15	0.00	0.00	0.65	0.80	0.15	19	19	0.16
0.5 %Au-0.5 %Pd/ZSM-5(280)	0.14	0.00	0.00	0.44	0.58	0.14	24	24	0.15

Methane oxidation reaction conditions: catalyst (0.028 g), H_2O (10.0 g), 435 psi total pressure (0.8 % H_2/1.6 % O_2/76.7 % CH_4/20.8 % N_2), 0.5 h, 50 °C, 1500 rpm. **Note:** Rates of H_2 conversion were found to be within experimental error of the blank reaction and therefore determination of H_2 selectivity could not be determined.

lower wavenumbers (2000–1800 cm^{-1}) are assigned to the multi-fold adsorption of CO onto contiguous Pd domains (*i.e.*, species adsorbed in a bidentate or tridentate manner). Across the catalytic series, a considerable variation in the proportion of the high-energy (isolated) and low-energy (contiguous) Pd sites was observed. Although it is important to highlight that it was not possible to quantify the relative populations of these species, it is considered that such analysis further evidences the key role of the nanoparticle carrier in controlling the nature of active metal species and in turn catalytic performance.

The role of Pd oxidation state in controlling catalytic activity towards the direct synthesis of H_2O_2 has been well studied, with the presence of domains of mixed Pd oxidation state suggested to be a key criterion in achieving enhanced catalytic efficacy, [26–28] although it is clear that other factors, including but not limited to, metal dispersion, nanoparticle composition and morphology as well as metal support interaction are also crucial in determining catalytic performance. Analysis of the supported AuPd catalysts by X-ray photoelectron spectroscopy (Table 2. and Figure S.4), reveals that the choice of catalyst support can significantly alter Pd speciation. Despite the exposure of all catalysts to a reductive thermal treatment (5 %H_2/Ar, 400 °C, 4 h, 10 °Cmin^{-1}), several catalyst formulations are found to consist of purely Pd^0 or Pd^{2+}, with others consisting of a mixture of both oxidation states. Notably, in the case of the 0.5 %Au-0.5 %Pd/CeO_2 catalyst, a considerable proportion of Pd was also found to exist as neither Pd^0 nor PdO, but rather as PdClx, further highlighting the key role of the support in controlling Pd speciation. The presence of mixed Pd oxidation state does partially correlate with catalytic performance towards H_2O_2 production and would identify the 0.5 %Au-0.5 %Pd/TiO_2 (95 $mol_{H2O2} kg_{cat}^{-1} h^{-1}$), 0.5 % Au-0.5 %Pd/$Al_2O_3$ (84 $mol_{H2O2} kg_{cat}^{-1} h^{-1}$) and 0.5 %Au-0.5 %Pd/Zeolite-Beta (119 $mol_{H2O2} kg_{cat}^{-1} h^{-1}$) formulations as effective H_2O_2 synthesis catalysts. Additionally, the fully metallic nature of the Pd species present in many of the ZSM-5-supported formulations would correlate well with the high activity of these formulations to catalyse H_2O_2 degradation. Indeed, previous studies have identified the low selectivity of Pd^0 towards H_2O_2 [29]. However, it is important to highlight the use of this metric alone as a predictor for catalyst performance would not be suitable. We further highlight that our XPS analysis was conducted on as-prepared samples alone, which is not fully representative of Pd oxidation states during the H_2O_2 direct synthesis reaction given the propensity of Pd^{2+} to reduce upon exposure to reaction conditions [30, 31].

Evaluation of the catalytic series toward the oxidation of methane, via *in situ* H_2O_2 production, is reported in Table 3, and a comparison of catalytic performance toward the *in situ* oxidation of methane and H_2O_2 synthesis is reported in Fig. 1 with an evaluation of catalyst stability, as indicated by metal leaching (determined via ICP-MS analysis of post-reaction solutions) reported in Table S.2. We wish to highlight the variation in reaction conditions used to evaluate catalytic performance towards H_2O_2 direct synthesis and methane oxidation, with the former utilising conditions optimised for H_2O_2 stability [23] and to allow for discernments in catalytic performance to be more easily made. Notably the H_2O_2 direct synthesis reaction utilises a CO_2 diluent (an *in situ* promoter of H_2O_2 stability) and a methanol co-solvent in order to inhibit competitive degradation reactions and improve reagent availability. With both CO_2 and methanol major products in the oxidative valorisation of methane, their utilisation in this reaction is not feasible.

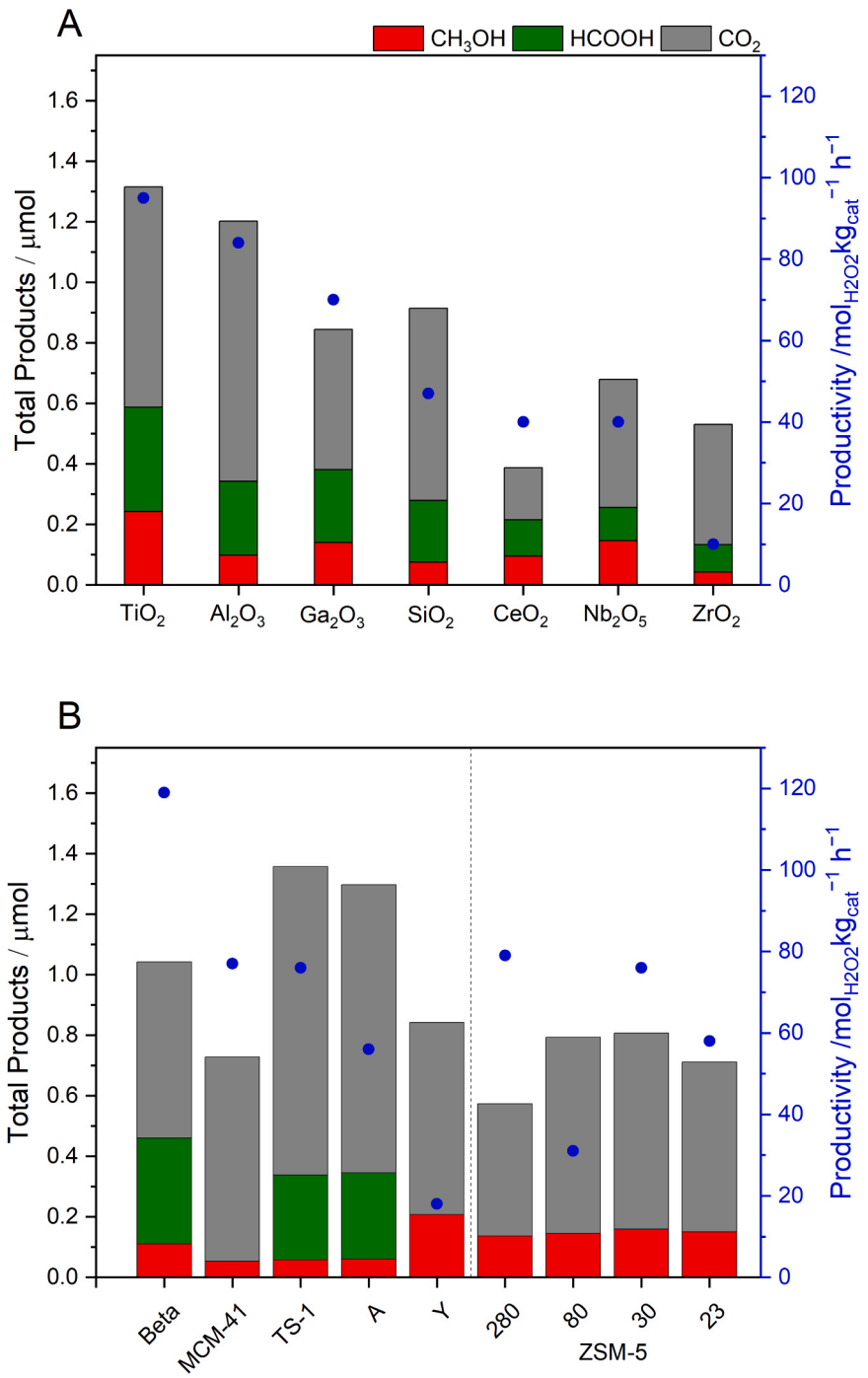

Fig. 1. A comparison of catalytic activity towards the direct synthesis of H_2O_2 and the oxidative valorisation of methane via *in situ* H_2O_2 production. **H_2O_2 direct synthesis reaction conditions:** Catalyst (0.01 g), H_2O (2.9 g), MeOH (5.6 g), 5 %H_2/CO_2 (420 psi), 25 %O_2/CO_2 (160 psi), 0.5 h, 2 °C, 1200 rpm. **Methane oxidation reaction conditions:** catalyst (0.028 g), H_2O (10.0 g), 435 psi total pressure (0.8 % H_2/1.6 % O_2/76.7 % CH_4/20.8 % N_2), 0.5 h, 50 °C, 1500 rpm.

However, it is clear that H_2O_2 synthesis rates, under methane activation conditions, will be limited and indeed improving catalytic selectivity towards H_2O_2 (*i.e.* avoiding H_2O formation), as well as rates of H_2O_2 production, are major challenges facing the commercial application of the *in situ* route to methane upgrading [9].

Importantly, no residual H_2O_2 was observed for any catalyst formulation, which may be attributed to a combination of (1) the poor stability of H_2O_2 even under the relatively mild reaction temperatures (50 °C) used in this study, (2) the lack of the carbonic acid promoter which is present in the H_2O_2 direct synthesis reaction (formed through the dissolution of the CO_2 gaseous diluent) and (3) the poor solubility of gaseous reagents (H_2 and O_2) in the reaction medium, in the absence of the alcohol co-solvents typically used to overcome this limitation in the case of H_2O_2 synthesis [32,33].

With previous studies highlighting the reactivity of analogous formulations towards methane oxidation [16] the reasonable performance of the 0.5 %Au-0.5 %Pd/TiO_2 catalyst (45 % oxygenate selectivity, 0.58 $\mu mol_{oxygenates} \mu mol_{metal}^{-1} h^{-1}$), is perhaps unsurprising. Interestingly, in the case of the oxide-supported catalysts, a clear relationship between individual reaction pathways was found, with the formulations that were most active towards H_2O_2 synthesis also yielding a greater concentration of oxygenates during methane upgrading. For the zeolitic sub-series, it

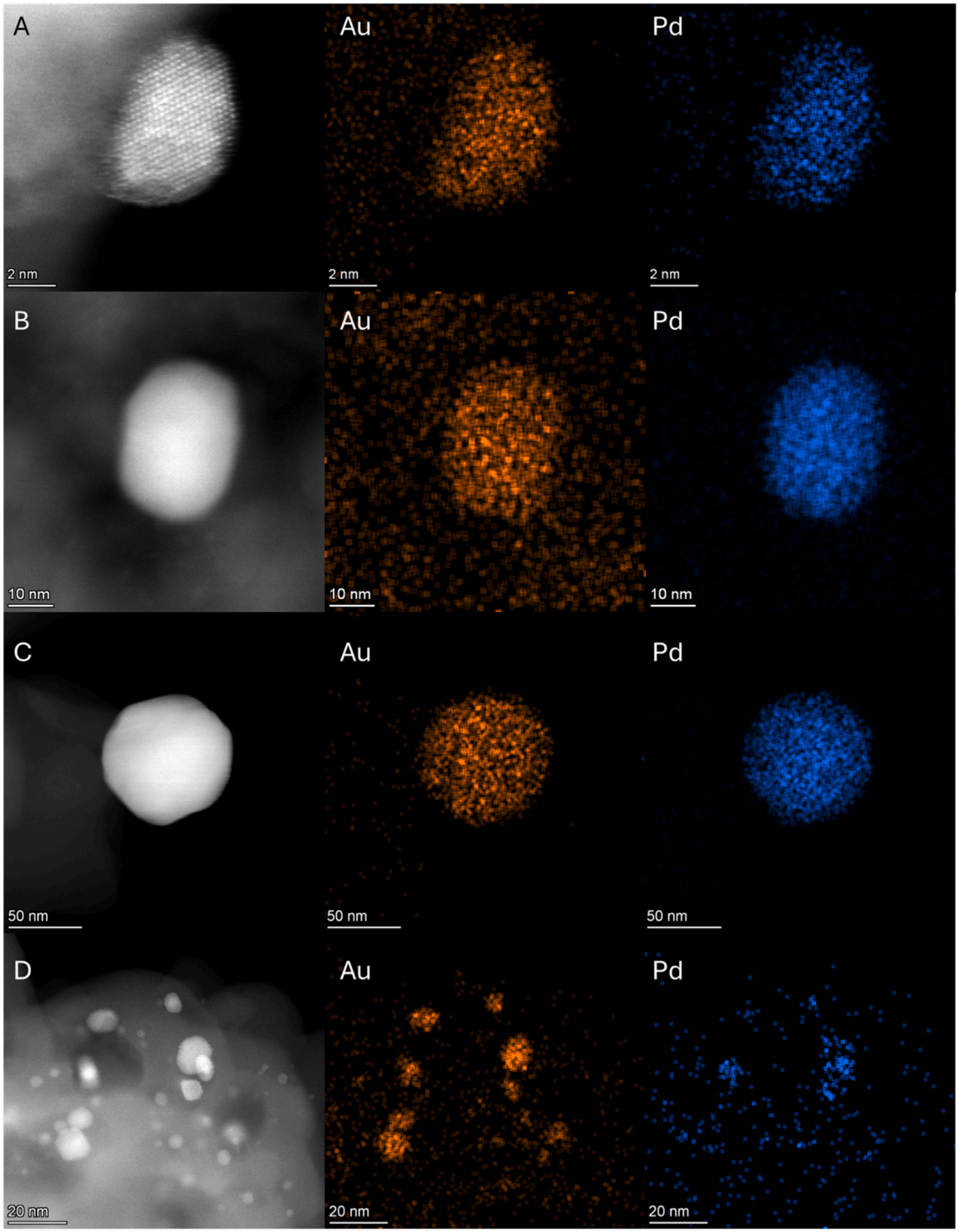

Fig. 2. HAADF-STEM and corresponding XED-S analysis of **(A)** 0.5 %Au-0.5 %Pd/TiO_2 **(B)** 0.5 %Au-0.5 %Pd/Zeolite-Beta **(C)** 0.5 %Au-0.5 %Pd/ZSM-5(30) and **(D)** 0.5 %Au-0.5 %Pd/TS-1 catalysts prepared via an excess chloride impregnation methodology. **Note**: all catalysts exposed to a reductive heat treatment (5 %H_2/Ar, 4 h 400 °C, 10 °Cmin^{-1}).

may have been predicted that the 0.5 %Au-0.5 %Pd/Zeolite-Beta catalyst would outperform alternative formulations (44 % oxygenate selectivity, 0.47 $\mu mol_{oxygenates} \mu mol_{metal}^{-1} h^{-1}$), based on the H_2O_2 synthesis activity alone. However, no clear correlation could be drawn between individual reaction pathways (*i.e.* H_2O_2 production and methane oxidation). When considered alongside recent reports that have identified the introduction of Au into Pd species to promote the release of oxygen-based radical species that are generated as intermediates in H_2O_2 synthesis (•OOH, •OH, $•O_2$), [15,17] such observations may indicate the contribution of alternative reactive oxygen species, beyond H_2O_2, towards the oxidative upgrading of methane.

Given the identical MFI framework structure of the TS-1 and ZSM-5 zeolites, in addition to the similar performance of this subset of catalysts towards H_2O_2 production, it is interesting to contrast the performance of

Table 4
Mean particle size of the as-prepared, supported AuPd catalysts, as determined by TEM.

Catalyst	Particle Size/nm (S.D)	Productivity / $mol_{H2O2}kg_{cat}^{-1}h^{-1}$	Productivity / $\mu mol_{oxygenates}\mu mol_{metal}^{-1}h^{-1}$
0.5 %Au-0.5 %Pd/TiO_2	5.4 (1.8)	95	0.58
0.5 %Au-0.5 %Pd/Zeolite-Beta	2.6 (0.7)	119	0.47
0.5 %Au-0.5 %Pd/ZSM-5 (30)	5.4 (3.2)	76	0.17
0.5 %Au-0.5 %Pd/TS-1	8.2 (5.9)	76	0.35

H_2O_2 direct synthesis reaction conditions: Catalyst (0.01 g), H_2O (2.9 g), MeOH (5.6 g), 5 %H_2/CO_2 (420 psi), 25 %O_2/CO_2 (160 psi), 0.5 h, 2 °C, 1200 rpm. **Methane oxidation reaction conditions:** catalyst (0.028 g), H_2O (10.0 g), 435 psi total pressure (0.8 % H_2/1.6 % O_2/76.7 % CH_4/20.8 % N_2), 0.5 h, 50 °C, 1500 rpm. **Note**: all catalysts exposed to a reductive heat treatment (5 %H_2/Ar, 4 h 400 °C, 10 °Cmin^{-1}).

this catalyst subset. The propensity of ZSM-5 based catalysts, when utilised with relatively high concentrations of preformed H_2O_2 to preferentially form formic acid over methanol has been previously reported by Hammond *et al.* and has been attributed to the surface decomposition of the methyl hydroperoxide intermediate to methanol and liberation of •OH radicals, which subsequently react with methanol to produce formaldehyde and formic acid [34]. Notably, our observations contrast those earlier studies, with methanol the only liquid product observed over the ZSM-5 subset of catalysts, whereas formic acid is the predominant liquid product in the case of the TS-1 supported catalyst. However, such trends may be rationalised given the relatively low reactivity of the catalysts studied within this work compared to those which have utilised commercial H_2O_2 as the oxidant.

Previous studies into AuPd-based catalysts prepared by a wet co-impregnation protocol have typically reported the presence of a bimodal particle size distribution, with nanoparticle morphology often dictated by the choice of gaseous atmosphere selected during thermal treatment, particularly when employing metal oxide supports. Indeed, exposure of such catalysts to oxidative heat treatments has been well reported to favour the formation of Au-core Pd-shell morphologies [35,36]. With a focus on key catalytic formulations (*i.e.* those formulations based on the TiO_2, Zeolite-Beta, TS-1 and ZSM-5 (30) supports), we subsequently employed high-angle annular dark-field scanning transmission electron microscopy (HAADF-STEM) alongside complimentary X-EDS analysis to investigate the role of the support in controlling both nanoparticle dispersion and morphology (Fig. 2, with additional data reported in Figure S.5, particle size distributions as determined by TEM are reported in Table 4 and Figure S.6). As in earlier studies, our analysis revealed the presence of both larger (>10 nm) and smaller (< 5 nm) species present in all formulations. However, distinct variations in nanoparticle population were observed across the catalyst series, with the 0.5 %Au-0.5 %Pd/TiO_2 formulation dominated by larger species, while the 0.5 %Au-0.5 %Pd/ZSM-5(30) analogue appears to consist predominantly of smaller species. Notably, the catalysts prepared on TS-1 and Zeolite-Beta contained a more equal distribution of both the smaller and larger species. Such analysis, particularly for the TiO_2 supported catalyst aligns well with our analysis by CO-DRIFTS (Figure S.3), which indicated the predominance of bridging CO species, indicative of contiguous Pd domains. Further investigation by XED-S established that for all formulations the metal nanoparticles exist predominantly as a well-mixed AuPd alloy, with the adoption of a random alloy morphology expected given the route to catalyst synthesis and the utilisation of a reductive heat treatment [20].

Interestingly, earlier investigations by Williams *et al.* [37] into the selective oxidation of methane using *ex situ* / commercially sourced H_2O_2 have highlighted the enhanced catalytic performance of larger AuPd nanoalloys. Based on these reports it may be possible to correlate catalyst performance towards *in situ* methane valorisation with nanoparticle size. However, attributing the observed catalytic trends to variation in nanoparticle dispersion alone is considered far too simplistic, particularly given the distinct variation in Pd oxidation state, another key factor in dictating catalyst performance, that we have identified across the catalyst series.

4. Conclusion

The oxidation of methane to methanol using *in situ* synthesised H_2O_2 is catalysed by a range of supported AuPd-based catalysts. The investigation of catalyst formulation, while maintaining total metal loading at 1 wt% and Au: Pd ratio of 1: 1 (wt/wt), revealed the crucial role of the catalyst supporting in dictating key catalytic properties, including the dispersion of active sites and electronic speciation of Pd, and in turn catalyst performance towards individual reaction pathways (*i.e.* H_2O_2 synthesis and *in situ* methane valorisation). Notably, in the case of the zeolite-supported materials, no clear correlation could be made between catalytic activity towards H_2O_2 synthesis and methane selective oxidation, which may indicate the contribution of alternative reactive oxygen species, such as •OH, $•O_2^-$ and •OOH, as well as H_2O_2 towards methane activation. While improvements in catalyst activity are clearly required, we consider that the materials investigated within this study represent a promising basis for further exploration for the selective oxidation of a range of feedstocks.

Author contributions

F.N. and R. J. L. conducted catalytic synthesis, testing and data analysis. F.N., R. J. L., A.L., D. J. M. and T. E. D. conducted catalyst characterisation and corresponding data processing. R. J. L., S.H.T and G. J. H. contributed to the design of the study. R. J. L., A.L., L.R.S., S.H.T and G. J. H. provided technical advice and result interpretation. R. J. L. wrote the manuscript and ESI, with all authors commenting on and amending both documents. All authors discussed and contributed to the work.

Funding

F.N. acknowledges the Chinese Scholarship Council for funding. R.J. L, A.L, L.R.S, S.H.T and G.J.H gratefully acknowledge Cardiff University and the Max Planck Centre for Fundamental Heterogeneous Catalysis (FUNCAT) for financial support.

CRediT authorship contribution statement

Graham J. Hutchings: Writing – review & editing, Supervision, Project administration, Funding acquisition, Formal analysis, Conceptualization. **Stuart H. Taylor:** Writing – review & editing, Visualization, Supervision, Project administration, Funding acquisition, Conceptualization. **Fenglou Ni:** Writing – review & editing, Methodology, Investigation, Formal analysis, Data curation. **Richard J Lewis:** Writing – review & editing, Writing – original draft, Visualization, Validation, Supervision, Project administration, Methodology, Investigation, Formal analysis, Data curation, Conceptualization. **Thomas E. Davies:** Writing – review & editing, Investigation, Formal analysis, Data curation. **David J. Morgan:** Writing – review & editing, Investigation, Formal analysis, Data curation. **Louise R. Smith:** Writing – review & editing, Formal analysis. **Ángeles López-Martín:** Writing – review & editing, Project administration, Formal analysis.

Declaration of Competing Interest

The authors declare that they have no known competing financial interests or personal relationships that could have appeared to influence the work reported in this paper.

Data Availability

Data will be made available on request.

Acknowledgements

XPS data collection was performed at the EPSRC National Facility for XPS ("HarwellXPS"), operated by Cardiff University and UCL, under contract no. PR16195. The authors would like to thank the CCI-Electron Microscopy Facility which has been part-funded by the European Regional Development Fund through the Welsh Government and The Wolfson Foundation.

Dedication

This paper is dedicated to Prof. David Jackson on the occasion of his retirement. The authors wish to thank David for his numerous contributions to the field and wish him a pleasant retirement.

Appendix A. Supporting information

Supplementary data associated with this article can be found in the online version at doi:10.1016/j.cattod.2024.114910.

References

[1] M. Ravi, M. Ranocchiari, J.A. vanBokhoven, Angew. Chem. Int. Ed. 56 (2017) 16464–16483.
[2] N.F. Dummer, D.J. Willock, Q. He, M.J. Howard, R.J. Lewis, G. Qi, S.H. Taylor, J. Xu, D. Bethell, C.J. Kiely, G.J. Hutchings, Chem. Rev. 123 (9) (2023) 6359–6411.
[3] R. Serra-Maia, F.M. Michel, T.A. Douglas, Y. Kang, E.A. Stach, A.C.S. Catal 11 (2021) 2837–2845.
[4] F. Ni, T. Richards, L.R. Smith, D.J. Morgan, T.E. Davies, R.J. Lewis, G.J. Hutchings, ACS Org. Inorg. Au. 3 (4) (2023) 177–183.
[5] J. Kang, E.D. Park, Catalysts 10 (2020) 299.
[6] E.D. Park, Y.-S. Hwang, C.W. Lee, J.S. Lee, Appl. Catal., A 247 (2003) 269–281.
[7] Á. Szécsényi, G. Li, J. Gascon, E.A. Pidko, ACS Catal. 8 (2018) 7961–7972.
[8] R. Serra-Maia, F.M. Michel, Y. Kang, E.A. Stach, A.C.S. Catal 10 (2020) 5115–5123.
[9] Z. Jin, L. Wang, E. Zuidema, K. Mondal, M. Zhang, J. Zhang, C. Wang, X. Meng, H. Yang, C. Mesters, F. Xiao, Science 367 (2020) 193–197.
[10] L. Kesavan, R. Tiruvalam, M.H.A. Rahim, M.I. bin Saiman, D.I. Enache, R. L. Jenkins, N. Dimitratos, J.A. Lopez-Sanchez, S.H. Taylor, D.W. Knight, C.J. Kiely, G.J. Hutchings, Science 331 (2011) 195–199.
[11] R.J. Lewis, K. Ueura, X. Liu, Y. Fukuta, T.E. Davies, D.J. Morgan, L. Chen, J. Qi, J. Singleton, J.K. Edwards, S.J. Freakley, C.J. Kiely, Y. Yamamoto, G.J. Hutchings, Science 376 (2022) 615–620.
[12] R.J. Lewis, G.J. Hutchings, Selective Oxidation Using, Acc. Chem. Res. 57 (2024) 106–119.
[13] A. Staykov, T. Kamachi, T. Ishihara, K. Yoshizawa, J. Phys. Chem. C. 112 (2008) 19501–19505.
[14] J. Li, T. Ishihara, K. Yoshizawa, J. Phys. Chem. C. 115 (2011) 25359–25367.
[15] T. Richards, J.H. Harrhy, R.J. Lewis, A.G.R. Howe, G.M. Suldecki, A. Folli, D. J. Morgan, T.E. Davies, E.J. Loveridge, D.A. Crole, J.K. Edwards, P. Gaskin, C. J. Kiely, Q. He, D.M. Murphy, J. Maillard, S.J. Freakley, G.J. Hutchings, Nat. Catal. 4 (2021) 575–585.
[16] M.H. AbRahim, M.M. Forde, R.L. Jenkins, C. Hammond, Q. He, N. Dimitratos, J. A. Lopez-Sanchez, A.F. Carley, S.H. Taylor, D.J. Willock, D.M. Murphy, C.J. Kiely, G.J. Hutchings, Angew. Chem. Int. Ed. 52 (2013) 1280–1284.
[17] C.M. Crombie, R.J. Lewis, R.L. Taylor, D.J. Morgan, T.E. Davies, A. Folli, D. M. Murphy, J.K. Edwards, J. Qi, H. Jiang, C.J. Kiely, X. Liu, M.S. Skjøth-Rasmussen, G.J. Hutchings, A.C.S. Catal 11 (2021) 2701–2714.
[18] T. Richards, R.J. Lewis, D.J. Morgan, G.J. Hutchings, Catal. Lett. 153 (2023) 32–40.
[19] E.N. Ntainjua, J.K. Edwards, A.F. Carley, J.A. Lopez-Sanchez, J.A. Moulijn, A. A. Herzing, C.J. Kiley, G.J. Hutchings, Green. Chem. 10 (2008) 1162–1169.
[20] M. Sankar, Q. He, M. Morad, J. Pritchard, S.J. Freakley, J.K. Edwards, S.H. Taylor, D.J. Morgan, A.F. Carley, D.W. Knight, C.J. Kiely, G.J. Hutchings, ACS Nano 6 (2012) 6600–6613.
[21] J. Brehm, R.J. Lewis, D.J. Morgan, T.E. Davies, G.J. Hutchings, Catal. Lett. 152 (2022) 254–262.
[22] J. Xu, R.D. Armstrong, G. Shaw, N.F. Dummer, S.J. Freakley, S.H. Taylor, G. J. Hutchings, Catal. Today 270 (2016) 93–100.
[23] A. Santos, R.J. Lewis, G. Malta, A.G.R. Howe, D.J. Morgan, E. Hampton, P. Gaskin, G.J. Hutchings, Ind. Eng. Chem. Res. 58 (2019) 12623–12631.
[24] J.J.K. Edwards, A. Thomas, B.E. Solsona, P. Lamdon, A.F. Carley, G.J. Hutchings, Catal. Today 122 (2007) 397–402.
[25] J. Lu, Z. Zhao, C. Xu, A. Duan, P. Zhang, J. Nat. Gas. Chem. 14 (2005) 213–220.
[26] X. Gong, R.J. Lewis, S. Zhou, D.J. Morgan, T.E. Davies, X. Liu, C.J. Kiely, B. Zong, G.J. Hutchings, Catal. Sci. Technol. 10 (2020) 4635–4644.
[27] A. Stenner, R.J. Lewis, J. Brehm, T. Qin, Á. López-Martín, D.J. Morgan, T.E. Davies, L. Chen, X. Liu, G.J. Hutchings, ChemCatChem 15 (2023) e202300162.
[28] D.W. Flaherty, ACS Catal. 8 (2018) 1520–1527.
[29] S.J. Freakley, Q. He, J.H. Harrhy, L. Lu, D.A. Crole, D.J. Morgan, E.N. Ntainjua, J. K. Edwards, A.F. Carley, A.Y. Borisevich, C.J. Kiely, G.J. Hutchings, Science 351 (2016) 965–968.
[30] A. Barnes, R.J. Lewis, D.J. Morgan, T.E. Davies, G.J. Hutchings, Catal. Sci. Technol. 12 (2022) 1986–1995.
[31] V.R. Choudhary, C. Samanta, T.V. Choudhary, Appl. Catal., A 308 (2006) 128–133.
[32] N.M. Wilson, D.W. Flaherty, J. Am. Chem. Soc. 138 (2016) 574–586.
[33] Q. Liu, J.C. Bauer, R.E. Schaak, J.H. Lunsford, Appl. Catal., A 339 (2008) 130–136.
[34] C. Hammond, M.M. Forde, M.H. AbRahim, A. Thetford, Q. He, R.L. Jenkins, N. Dimitratos, J.A. Lopez-Sanchez, N.F. Dummer, D.M. Murphy, A.F. Carley, S. H. Taylor, D.J. Willock, E.E. Stangland, J. Kang, H. Hagen, C.J. Kiely, G. J. Hutchings, Angew. Chem. Int. Ed. 51 (2012) 5129–5133.
[35] A.A. Herzing, M. Watanabe, J.K. Edwards, M. Conte, Z.R. Tang, G.J. Hutchings, C. J. Kiely, Faraday Discuss. 138 (2008) 337–351.
[36] J.K. Edwards, A.F. Carley, A.A. Herzing, C.J. Kiely, G.J. Hutchings, Faraday Discuss. 138 (2008) 225–239.
[37] C. Williams, J.H. Carter, N.F. Dummer, Y.K. Chow, D.J. Morgan, S. Yacob, P. Serna, D.J. Willock, R.J. Meyer, S.H. Taylor, G.J. Hutchings, ACS Catal. 8 (2018) 2567–2576.